

DNA Transport and Delivery in Thermal Gradients near Optofluidic Resonators

Xavier Serey,¹ Sudeep Mandal,^{1,*} Yih-Fan Chen,^{2,3,†} and David Erickson^{3,‡}

¹*School of Applied and Engineering Physics, Cornell University, Ithaca, New York 14853, USA*

²*Kavli Institute at Cornell for Nanoscale Sciences, Cornell University, Ithaca, New York 14853, USA*

³*Sibley School of Mechanical and Aerospace Engineering, Cornell University, Ithaca, New York 14853, USA*

(Received 29 July 2011; published 27 January 2012)

Heat generation and its impact on DNA transport in the vicinity of an optofluidic silicon photonic crystal resonator are studied theoretically and experimentally. The temperature rise is measured to be as high as 57 K for 10 mW of input power. The resulting optical trapping and biomolecular sensing properties of these devices are shown to be strongly affected by the combination of buoyancy driven flow and thermophoresis. Specifically, the region around the electromagnetic hot spot is depleted in biomolecules because of a high free energy barrier.

DOI: [10.1103/PhysRevLett.108.048102](https://doi.org/10.1103/PhysRevLett.108.048102)

PACS numbers: 87.15.Vv, 42.60.Da, 42.62.Be, 47.61.-k

Nanoscale optofluidic resonators have recently proven themselves useful in fields ranging from chemical and biological sensing [1] to nanomanipulation [2,3]. In most of these optofluidic devices, the transport of solutes to the electromagnetic hot spot is critical to the device's performance. The effects of hydrodynamic forces on trapping experiments have been characterized [4,5], as well as the effect of plasmonic heat sources on the fluid flow [6]. In the past few years, the transport of molecules due to temperature gradients, often called thermophoresis [6,7], has been shown to be an important phenomenon in molecular transport [8]. Recently, researchers have studied the effects of thermophoresis on plasmonic based sensing [9]. While the absorption of infrared light by water in the evanescent field of silicon photonic devices is expected to produce local heating, there is currently only a weak understanding of the magnitude of the effect and how it would affect the transport of molecules in the context of optical nanotweezing and silicon photonic biosensing.

Here, we aim at demonstrating the effects of the optical absorption of water in the infrared on temperature, flow dynamics, and λ DNA transport in the vicinity of a silicon photonic crystal (PC) resonator. The temperature rise at the PC resonator leads to buoyancy forces that pinch the flow around the resonator while thermophoretic drift can either expel or attract particles from the resonator according to the signs of their thermophoretic coefficient. As in any thermophoretic event, the transport properties are strongly dependent on the species, medium, and temperatures considered [6]. In this Letter, we first examine the heat generation and temperature field around the photonic cavity pointing out which parameters most significantly affect heat generation. We then study the flow around the cavity and the particle transport properties of λ DNA. The 48 kbp λ DNA is a molecule of particular interest due to its biophysical applications and whose thermophoretic properties have been characterized [6], additionally it has already been trapped by photonic devices [3]. Finally, we use thermodynamics

and reaction rate theory to provide a new understanding on how significantly common experiments, such as trapping, are likely to be affected by the heat production.

The photonic crystal (PC) resonators used in this study are standing wave resonators formed by the insertion of a periodic array of holes into a silicon waveguide. These holes surround a central cavity consisting of the bare silicon waveguide and, in some cases, an extremely small central hole as in Fig. 1(a). Discrete modes can exist in the cavity constituting a simple and effective optical trap [10] and sensor [11]. Because the electromagnetic field is enhanced, the improved interaction with the solution results in a temperature increase which can be measured *in situ*. The devices were fabricated with standard *e*-beam fabrication procedures on a 250 nm silicon-on-insulator wafer. The experimental setup in this work consists of the silicon chip containing the photonic elements on top of which is assembled a transparent microfluidic channel. The ensemble is mounted on a microscope stage.

First numerical and experimental studies of the temperature increase near the photonic crystal resonator were performed. At the working wavelength of 1550 nm, water absorbs more than the optical materials present [12], so in our simulations all of the imaginary permittivities were ignored except for water ($\epsilon'' = 3.51 \times 10^{-4}$ [13]). The electromagnetic to heat energy conversion was first computed numerically solving Maxwell's equations and used as a source term in the diffusive heat equation for a channel geometry of 500 μm wide, 125 μm high. Convective effects were numerically verified to be negligible as expected from the low Péclet number $\text{Pe} < 10^{-3}$. As seen in Eq. (1), the power lost to heat is proportional to the electromagnetic energy density and to the power input. The simulations are performed for 10 mW of power input, a commonly used power in experiments.

$$\kappa \nabla^2 T = \frac{\omega}{2} \text{Im}(\epsilon) \times |\mathbf{E}|^2(\vec{r}). \quad (1)$$

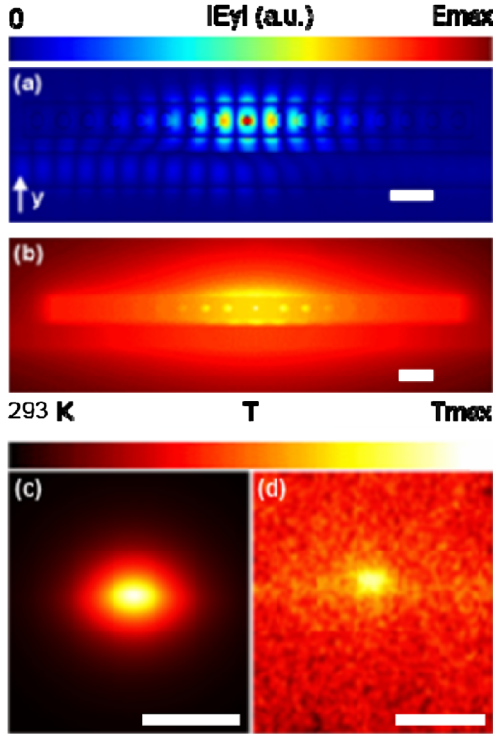


FIG. 1 (color online). Scale bars: 500 nm (a),(b), 15 μm (c), (d). (a) Modulus of E_y in a PC resonator with a central hole. The light is coupled from the bottom waveguide. (b) Numerical estimation of the temperature increase of a PC resonator with a central hole. The maximum temperature is 350 K. (c) Numerical estimation of the temperature 2 μm above the resonator. For 1.7 mW of power input, the maximum temperature reached is 4 K. (d) Fluorescently measured temperature increases for 1.7 mW of estimated power input, 2 μm above the surface of the resonator. The maximum temperature increase is 4.8 K after correction for bleaching and thermophoresis of the rhodamine *B*.

Here, T is the temperature, κ is the thermal conductivity of the material, ω is the resonant frequency, ϵ is the permittivity, and \mathbf{E} is the electric field. In thin silicon beams, phonons-surface interactions cause the conductivity to change as compared to bulk silicon, this was taken into account by setting $\kappa = 100 \text{ W m}^{-1}\text{K}^{-1}$ [14]. It was found that the maximum temperature increases is 57 K for cavities with a central hole as plotted in Fig. 1(b).

In the central hole, the superposition of evanescent fields allows for a high field enhancement [3]. The field intensity's full strength interacts with the water leading to a particularly high temperature increase there. Experimentally, temperature sensitive fluorescent dye Rhodamine *B* was used to measure the temperature 2 μm above the resonator. Correcting for the imaging defects, Fig. 1(d) was obtained. The maximum temperature increase measured of $4.8 \pm 1 \text{ K}$. The measurement was carried out at an estimated power input into the resonator of $1.7 \pm 0.3 \text{ mW}$. The numerical code took bleaching into

account whereas the correction for thermophoresis was inferred from the experimental results published by Cordero *et al.* [15]. The measured temperature increase is 20% higher than the predicted 4 K increase for 1.7 mW of power input [Fig. 1(c)]. The agreement offered validation of the theoretical calculation. Details of these experiments are provided in the Supplemental Material [16].

Following the thermal characterization, the transport properties of species near the PC resonator were examined. Numerical simulations were carried out to solve the steady state incompressible Navier-Stokes equation in the microfluidic environment [Eq. (2)]. The effect of the thermal nonequilibrium was accounted for using the Boussinesq approximation [Eq. (3)]. The validity of the Boussinesq approximation here is justified by the extremely low Grashoff and Rayleigh numbers in 10 μm high microfluidic channels [17]. The Grashoff number is defined as $\text{Gr} = g\beta(T_m - T_0)D_h^3/\nu^2 < 10^{-3}$ and the Rayleigh number is $\text{Ra} = g\beta(T_m - T_0)D_h^3/\nu\alpha < 10^{-3}$ [16]. Here, g is the standard gravity, β , ν , and α , are the thermal expansion coefficient, kinematic viscosity, and thermal diffusivity of water, respectively. T_m and T_0 are the maximum and ambient temperature, and D_h is the hydraulic radius.

$$\rho \mathbf{u} \cdot \nabla \mathbf{u} = -\nabla p + \mu \nabla^2 \mathbf{u} + \mathbf{f}, \quad (2)$$

$$\mathbf{f} = -\mathbf{g}(\rho(T) - \rho(T_0)). \quad (3)$$

In these equations, \mathbf{u} is the flow speed, p the pressure, ρ and μ are the density and viscosity of water, \mathbf{g} is the standard gravity, and \mathbf{f} is the Boussinesq buoyancy term. The result of these simulations is detailed in the Supplemental Material [16]. λ DNA is often used as flow tracer because it follows the streamlines at steady state. However, in the presence of temperature gradients, their velocity needs to be corrected for thermal drift [6]. Thermophoresis is the movement of particles induced by temperature gradients, as expressed in Eq. (4). After correcting the flow streamlines for thermophoresis, we obtain actual path lines followed by DNA molecules. As can be seen, the path lines avoid the resonator and the region behind it is depleted (Fig. 2 and Supplemental Material [16]). Also importantly, the path lines feature stop points behind the resonator where the λ DNA is trapped due to the opposition of the thermal drift and the fluid flow. This effect was demonstrated as a molecule trap by Duhr *et al.* [18]. The peculiar accumulation and depletion are best expressed in terms of concentration profile. The steady state concentration profile was computed as the solution of the convection-diffusion equations (5) corrected for thermophoretic flow:

$$\mathbf{u}_T = -D_T \nabla T, \quad (4)$$

$$\nabla \cdot (c(\mathbf{u} + \mathbf{u}_T) - D \nabla c) = 0. \quad (5)$$

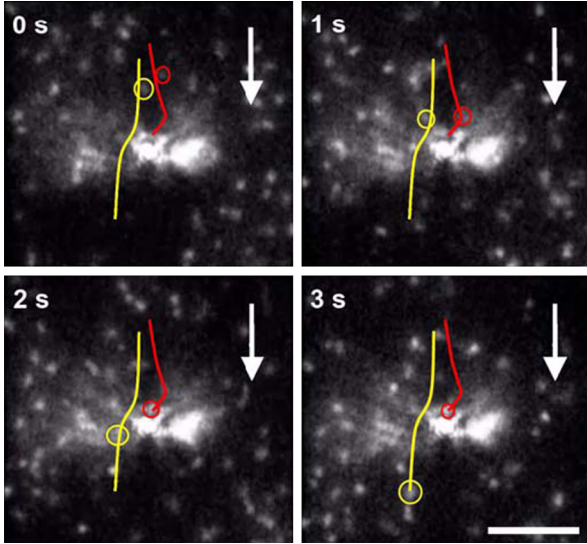


FIG. 2 (color online). Times steps showing λ DNA transport near the optical resonator (bright central light). The white arrow represents the direction of the flow. The flow rate is $12\,500\ \mu\text{m}^3/\text{s}$. One molecule contours the photonic crystal (yellow online), while one is thermally trapped (red online). Images taken from video in Supplemental Material (rotated 90°) [16]. Scale: $50\ \mu\text{m}$.

Here, c is the concentration, \mathbf{u} the velocity profile imported from the Navier-Stokes solution, \mathbf{u}_T is the thermophoretic flow, and D and D_T are the diffusion coefficients and the thermophoretic coefficient ($0.8\ \mu\text{m}^2\text{s}^{-1}$ and $0.9\ \mu\text{m}^2\text{s}^{-1}\text{K}^{-1}$, respectively, measured for 48 kbp λ DNA in 1 mM Tris at 20°C by Duhr *et al.* [6]).

Experimentally, the concentration profile was measured from flowing λ DNA (Fig. 2) in 1 mM Tris, 1 mM NaCl, buffer at $12\,500\ \mu\text{m}^3/\text{s}$ around a 1D photonic crystal resonator that was excited at the resonant frequency. The time-integrated intensity at each pixel was related to the concentration profiles under an ergodic assumption. A comparison of the experimental concentration profile with the numerical result is presented in Fig. 3. The concentration profile is shown to be consistent with simulations. In particular, as predicted from the simulation, the concentration profile exhibits an accumulation region in front of the resonator. Both numerically and experimentally, we observe a threefold increase ($c_{\text{exp}}/c_0 = 3.2 \mp 0.28$, $c_{\text{num}}/c_0 = 2.9$) of the concentration at the thermal trap. A depletion region behind the resonator is also visible experimentally and numerically ($c_{\text{exp}}/c_0 = 0.87 \mp 0.05$, $c_{\text{num}}/c_0 = 0.7$, $25\ \mu\text{m}$ behind the resonator). Differences between the calculated profile and the experimental profile are accounted for by the experimental method (background fluorescence from molecules out of focus, averaging in the Z direction over the depth of field, and variations in flow speed and coupled power) and by the numerical assumption that the thermophoretic coefficient is temperature independent [19]. As the thermophoretic

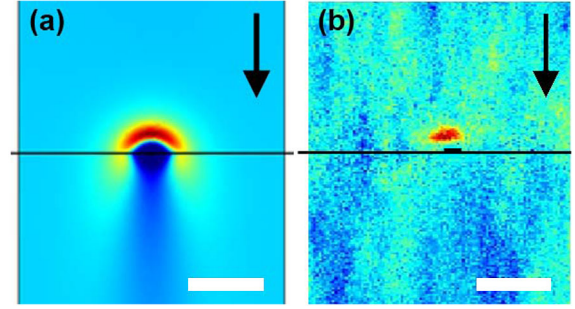


FIG. 3 (color online). (a) Numerical (b) and experimental concentration profile in the vicinity of a PC resonator with a central hole. The power input is $10 \pm 1\ \text{mW}$, and the flow is oriented top down at $12\,500\ \mu\text{m}^3/\text{s}$. The red spot corresponds to the thermophoretic trap due to opposed thermal and convective flows. Black lines: feeding waveguides. Black arrow represents the direction of the flow. Scale bars: $25\ \mu\text{m}$.

coefficients tend to increase with temperature, a higher than calculated accumulation was to be expected. It is important to note that although there is an accumulation in advance of the resonator, this effect significantly reduces species transport to the electromagnetic hot spot. It would therefore negatively impact biomolecular sensing and optical trapping.

In the presence of thermal effects and drag forces, the free energy is evaluated by the means of Eq. (6) wherever the local equilibrium condition $\nabla T \leq (a \times D_T/D)^{-1}$ is met [6], with the hydrodynamic radius (Supplemental Material [16]).

$$c(\mathbf{r}) = c_0 e^{-F(\mathbf{r})/k_B T}. \quad (6)$$

In this equation c is the steady state concentration, c_0 is the bulk concentration, $F(\mathbf{r})$ and $k_B T$ are the total free energy and the thermal energy fluctuation at the position \mathbf{r} , respectively. As seen in the concentration profile, this thermochemical free energy leads to a minimum where molecules accumulate [Fig. 4(b)]. At the resonator, the free energy is the highest for molecules with positive thermophoretic coefficient, such as λ DNA, which are therefore repelled. To this free energy, we must add the electromagnetic potential created by the photonic trap. The electromagnetic hot spot is the global minimum of the potential energy and therefore a stable position for molecules. The thermochemical free energy barrier is as high as $12k_B T$ for 10 mW of power input and spans a few micrometers range whereas the electromagnetic potential well is very deep in comparison (thousands of $k_B T$) but spanning a range of a few hundred nanometers. The resulting superposition is sketched in Figs. 4(a) and 4(b). The absolute minimum of the potential energy, the electromagnetic well, is surrounded by a free energy barrier. The metastable minimum, which is the thermal accumulation point, is accessible to the molecules of the solution as it is not surrounded by a potential barrier. Last, entropic free energies should be added when confining macromolecules

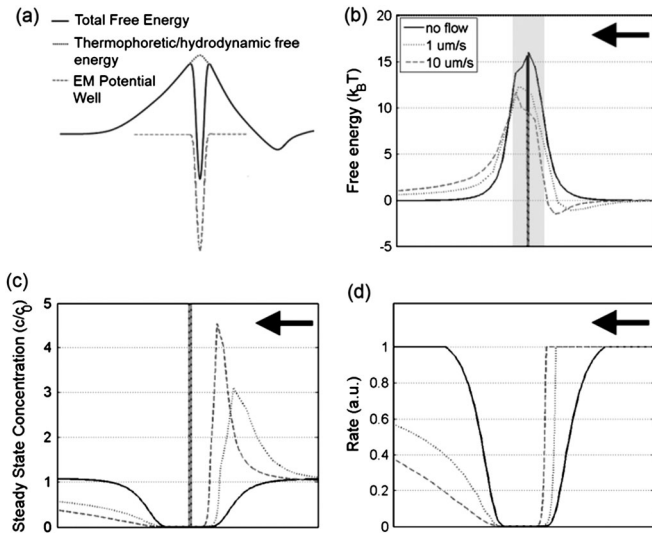


FIG. 4. (a) Sketch of the superposition of the free energy resulting from the thermodiffusion and the electromagnetic well. (b)–(d) Numerical estimations along the flow direction (Y direction, horizontal scale: $-50 \mu\text{m}$ to $50 \mu\text{m}$, volumetric flow rate $12\,500 \mu\text{m}^3/\text{s}$) for 10 mW of power input. The legend in (b) applies to (c),(d) as well. (b) Free energy diagram in $k_B T$ units. At the resonator, the electromagnetic potential well is added to the free energy. The EM potential well is much deeper than the free energy barrier but spans a smaller region. The potential barrier is about $12k_B T$. The arrow represents the flow direction. The gray area represents the region where the local equilibrium criteria is not met; hence, the free energy expansion [Eq. (6)] is less accurate (Supplemental Material [16]). (c) Concentration profile. Even with no superimposed flow, we notice a small accumulation in the vicinity of the resonator. This is the result of the buoyancy induced convective flow (Supplemental Material [16,22]). (d) Diffusion rate estimated from the energy barrier through (7). At the resonator, the rate is $1/3\,000\,000$ times the average diffusion time.

in small spaces [20], but have been ignored here when compared to the electromagnetic potential. Flow drag tends to pull particles out of the trap but is also negligible for traps of hundreds of $k_B T$ [5].

In the steady state, the concentration profile is related to the energy profile by the Boltzmann distribution (6), where the two metastable states are populated [Fig. 4(c)]. The depth of the electromagnetic well is weakly affected by the free energy; therefore, the trapping remains very stable and steady state population of the optical trap should remain high. In the presence of the thermal field, the optical trap is now surrounded by an energy barrier. The reaction rate theory provides valuable information about the dynamical picture. Reaction rates theory relates the energy barrier in the context of reaction kinetics [21] to the reaction rate as first explained by Kramers and seen in Eq. (7).

$$k(\mathbf{r}) = 2\pi k_0 e^{-\Delta F(\mathbf{r})/k_B T} \quad (7)$$

Here, k is the trap or escape rate, k_0 is the reference trap or escape rate, and ΔF is the energy barrier. The 2π factor

comes from the integration over the upper half sphere. For a molecule to be trapped optically, it first needs to tunnel through the energy barrier, leading to a very low trap rate [Fig. 4(d)]. In trapping experiments, for molecules with high thermophoretic coefficient, the average trapping time is evaluated as the inverse of the trapping rate. From 4(d), the average time for a molecule to diffuse into the optical trap is $3\,000\,000$ times longer than to be thermally trapped. The energy barrier's height was numerically found to be proportional to the factor $S_T P_{\text{in}}$. The Soret coefficient S_T is defined as the ratio of D_T/D . The term P_{in} is the laser power input. By linearity of the wave and heat equations, the temperature increase is proportional to the power input as long as heat conduction dominates convection. Under this condition and as long as the Soret coefficient can be considered to be independent of temperature, the former result holds. This result is intuitive from an energy standpoint when the local equilibrium condition is met.

In conclusion, we have studied the effect of heat generation on the transport of solutes to an optical resonator. Thermophoresis was found to play an important role in particle transport near the resonator significantly reducing the local concentration at the electromagnetic hot spot, thereby negatively affecting the performance of these devices as biomolecular sensors. These effects were further explained in thermodynamic terms using the formalism of reaction kinetics. These results should pave the way for new designs of optofluidic nanotweezers and biosensors that will avoid thermal effects or take advantage of them.

Elements of this work were funded by the U.S. NSF (No. 0708599), U.S. Department of Energy (DE-SC0003935), and U.S. NIH (1R21EB009202). Y.F.C. was partially supported by a postdoctoral fellowship from the Kavli Institute at Cornell for Nanoscale Sciences.

*Present address: GE Global Research, KWC1426, One Research Circle, Niskayuna, NY 12309, USA.

†Present address: Department of Biomedical Engineering, National Cheng Kung University, Tainan 701, Taiwan.

‡de54@cornell.edu

- [1] H. K. Hunt and A. M. Armani, *Nanoscale* **2**, 1544 (2010).
- [2] D. Erickson, X. Serey, Y.-F. Chen, and S. Mandal, *Lab Chip* **11**, 995 (2011).
- [3] A. H. J. Yang, S. D. Moore, B. S. Schmidt, M. Klug, M. Lipson, and D. Erickson, *Nature (London)* **457**, 71 (2009).
- [4] K. Khosla, J. D. Swaim, J. Knittel, and W. P. Bowen, [arXiv:1011.3897v1](https://arxiv.org/abs/1011.3897v1).
- [5] A. H. J. Yang and D. Erickson, *Nanotechnology* **19**, 045704 (2008).
- [6] S. Duhr and D. Braun, *Proc. Natl. Acad. Sci. U.S.A.* **103**, 19678 (2006).
- [7] A. Wurger, *Rep. Prog. Phys.* **73**, 126601 (2010).
- [8] A. Hammack, Y.-L. Chen, and J. K. Pearce, *Phys. Rev. E* **83**, 031915 (2011); D. Vigolo, S. Buzzaccaro, and R. Piazza, *Langmuir* **26**, 7792 (2010).

- [9] T. Kang, S. Hong, Y. Choi, and L. P. Lee, *Small* **6**, 2649 (2010).
- [10] X. Serey, S. Mandal, and D. Erickson, *Nanotechnology* **21**, 305202 (2010).
- [11] S. Mandal and D. Erickson, *Opt. Express* **16**, 1623 (2008).
- [12] T. Asano, B. S. Song, and S. Noda, *Opt. Express* **14**, 1996 (2006).
- [13] G. M. Hale and M. R. Querry, *Appl. Opt.* **12**, 555 (1973).
- [14] K. E. Goodson and Y. S. Ju, *Annu. Rev. Mater. Sci.* **29**, 261 (1999).
- [15] M. L. Cordero, E. Verneuil, F. Gallaire, and C. N. Baroud, *Phys. Rev. E* **79**, 011201 (2009).
- [16] See Supplemental Material at <http://link.aps.org/supplemental/10.1103/PhysRevLett.108.048102> for the movie of the experiment presented in Fig. 2, details about the experimental setup, and the numerical work.
- [17] D. D. Gray and A. Giorgini, *Int. J. Heat Mass Transf.* **19**, 545 (1976).
- [18] S. Duhr and D. Braun, *Phys. Rev. Lett.* **97**, 038103 (2006).
- [19] S. Iacopini, R. Rusconi, and R. Piazza, *Eur. Phys. J. E* **19**, 59 (2006).
- [20] J. Han and H. G. Craighead, *Science* **288**, 1026 (2000).
- [21] H. Grabert, *Phys. Rev. Lett.* **61**, 1683 (1988).
- [22] J. S. Donner, G. Baffou, D. McCloskey, and R. Quidant, *ACS Nano* **5**, 5457 (2011).